Research Article

Synthesis and Characterization of $BiVO_4$/S,N-CQDs as Photoelectrochemical Water Splitting Material

Herlina Arthaningtyas and Nonni Soraya Sambudi*
Chemical Engineering Department, Universitas Pertamina, Simprug, Kec. Kby. Lama, Kota Jakarta Selatan, DKI Jakarta, Indonesia

Liszulfah Roza
Research Center for Nanotechnology Systems, National Research and Innovation Agency (BRIN), Jl. Raya Serpong, Muncul, Kec. Setu, Kota Tangerang Selatan, Banten, Indonesia

Vivi Fauzia
Department of Physics, Faculty of Mathematics and Natural Sciences, Universitas Indonesia, Depok, Indonesia

Suriati Sufian
Department of Chemical Engineering, Universiti Teknologi PETRONAS, Seri Iskandar, Perak, Malaysia

Sylvia Ayu Pradanawati and Yose Fachmi Buys
Department of Mechanical Engineering, Faculty of Industrial Technology, Universitas Pertamina, Simprug, Kec. Kby. Lama, Kota Jakarta Selatan, DKI Jakarta, Indonesia

Resista Vikaliana
Department of Logistic Engineering, Faculty of Industrial Technology, Universitas Pertamina, Simprug, Kec. Kby. Lama, Kota Jakarta Selatan, DKI Jakarta, Indonesia

* Corresponding author. E-mail: nonni.ss@universitaspertamina.ac.id DOI: 10.14416/j.asep.2025.05.006
Received: 9 December 2024; Revised: 20 January 2025; Accepted: 19 February 2025; Published online: 23 May 2025

Abstract
Hydrogen has emerged as a promising renewable energy source to replace fossil fuels, driving the need for efficient and low-emission hydrogen production methods. Among these, photoelectrochemical (PEC) water splitting using solar energy and semiconducting materials as photoanodes holds significant potential. This study focuses on enhancing the performance of *bismuth vanadate* ($BiVO_4$), a highly promising photoanode material, synthesized on *fluorine-doped tin oxide* (FTO) substrates via a hydrothermal method. This research aims to improve the efficiency and stability of $BiVO_4$ as a photoelectrochemical anode material by integrating sulfur-nitrogen-doped carbon quantum dots (S,N-CQDs), derived from *Egeria densa algae*, to minimize charge recombination and enhance light absorption as well as the efficiency of solar energy conversion to hydrogen. To address the challenge of charge recombination, S,N-CQDs were integrated into $BiVO_4$ using a spray-coating method in varying volumes (0, 2.5, 5, 7.5, and 10 mL). The incorporation of S,N-CQDs significantly reduced the band gap of $BiVO_4$, with the most notable reduction at 7.5 mL (from 3.14 eV to 2.70 eV). This modification resulted in enhanced PEC water splitting performance, with a maximum photocurrent density of 0.0698 mA/cm² and a photoconversion efficiency of 0.0131%. Additionally, the optimized $BiVO_4$/S,N-CQDs photoanode exhibited a double-layer capacitance (Cdl) of 0.102 mF/cm², indicating improved charge transport properties. These results demonstrate that the integration of S,N-CQDs into $BiVO_4$ not only enhances PEC efficiency but also contributes to the development of cost-effective, sustainable solutions for solar-driven hydrogen production, supporting the transition to a renewable energy future.

Keywords: $BiVO_4$, Egeria densa algae, Hydrothermal method, PEC water splitting, S,N-CQDs

1 Introduction

The international is presently going through an environmental disaster exacerbated via way of means of the developing international call for electricity. Fossil fuels nevertheless account for 83% of the worldwide electricity supply, which is regarded as their combustion ends in giant carbon emissions, thereby contributing notably to environmental degradation and weather change [1]. Hydrogen holds significant potential for large-scale energy storage due to its high energy density of around 143 MJ/kg and its ability to be used with fuel cells for backup power generation. One of its key blessings is its use in zero CO_2 emissions, permitting extra hydrogen to be saved for destiny use as the gas inside the hydrogen economy. Furthermore, as compared to different principal electricity garage technologies, along with lithium-ion batteries, hydrogen gives extra favorable cradle-to-grave characteristics, as it's far non-toxic, in contrast to the acidic chemistry of lithium-ion batteries presently in use [2]. Several technologies have been explored to decorate renewable electricity garages, consisting of pumped hydroelectric energy, compressed air electricity garages, lithium-ion batteries, and hydrogen. Hydrogen, in particular, may be produced through numerous methods, consisting of thermo-chemical, electrochemical, photochemical, photocatalytic, and photo-electrochemical processes [3].

Photoelectrochemical (PEC) water splitting is considered a promising, eco-friendly, and sustainable method. It correctly converts sun electricity into chemical electricity, allowing the transformation of water into precious products, with hydrogen being one of the key outputs [4]. PEC reactions are endothermic and need a Gibbs free energy of $\Delta G_{(298°)} = 237$ kJ/mol, which corresponds to a potential of $\Delta E° = 1.23$ V per electron transferred. To effectively utilize semiconductors and light energy in the PEC process, the semiconductor material must be capable of absorbing photons with an energy of at least 1.23 eV (equivalent to wavelengths of 1000 nm or shorter) and converting this energy into the production of hydrogen and oxygen [5].

The main process in PEC cells involves three key stages: 1) the generation of charge carriers, which occurs when light is absorbed by the photoanode (semiconductor material) with energy greater than its band gap, resulting in the creation of electrons and holes; 2) the separation and transfer of these charges to the semiconductor-electrolyte interface; and 3) the oxygen evolution reaction (OER), which takes place at the holes on the semiconductor surface, and the hydrogen evolution reaction (HER), where electrons travel to the cathode surface via a conductive wire, reducing protons to produce hydrogen gas [6].

Photoanodes are typically made from semiconductor materials, like $BiVO_4$ (*Bismuth Vanadate*), an n-type semiconductor with a band gap of approximately 2.4 eV. $BiVO_4$ is considered a promising candidate for PEC water-splitting applications due to its non-toxic nature, affordability, stability, and ability to absorb visible light [7]. However, there are still some challenges to overcome. To address problems such as poor electron transport and slow oxidation kinetics, various strategies have been applied to enhance the PEC performance of $BiVO_4$ as a photoanode. These strategies involve creating heterostructure catalysts like $WO_3/BiVO_4$ and $SnO_2/BiVO_4$, as well as doping $BiVO_4$ with transition metals such as W and Mo, which have been shown to improve electron transport and, in turn, increase the efficiency of PEC water splitting [8]. Recently, carbon quantum dots (CQDs) have emerged as promising materials for enhancing the performance of semiconductors in photoelectrochemical (PEC) water splitting applications due to their high UV light absorption, wide visible light absorption range, and efficient charge carrier transport properties. They also act as co-catalysts, improving the oxygen evolution reaction (OER) and boosting overall PEC system performance. $BiVO_4$, despite its good light absorption ability, suffers from high electron-hole pair recombination rates, limiting charge transfer efficiency. The incorporation of S,N-CQD significantly mitigates this limitation by creating electronic defects, leading to increased photocurrent density and enhanced PEC efficiency [9]. The addition of heteroatoms such as nitrogen (N), sulfur (S), oxygen (O), and phosphorus (P) through doping or co-doping can greatly enhance the fluorescence intensity and luminescent properties of carbon quantum dots (CQDs). This improvement in the optical properties of CQDs is attributed to the similar atomic size and electronegativity between carbon and the dopant ions, which foster better electronic interactions and enhance their fluorescence characteristics [10]–[12].

$BiVO_4$ exists in four distinct crystal forms or polymorphs: monoclinic scheelite, tetragonal scheelite, tetragonal zircon, and orthorhombic. The natural form of $BiVO_4$, known as *pucherite*, has an orthorhombic crystal structure. While the orthorhombic phase is most found in nature, it presents

difficulties for laboratory synthesis. Consequently, $BiVO_4$ synthesized in the lab typically adopts either the scheelite or zircon structures, rather than the naturally occurring pucherite form [13].

Egeria densa is an aquatic plant that can adapt to low CO_2 conditions by developing special mechanisms to increase photosynthetic efficiency, in other words, it can help reduce CO_2 concentration in the atmosphere [14], [15]. It features irregularly branched stems, typically 1 to 3 mm in diameter, and can grow over 3 meters long. The plant has leaves and branches that develop along 0 to 15 internodes, with lengths ranging from 2.5 mm to 24 mm. Its leaves generally measure 1 to 3 cm in length and can reach widths of up to 5 mm. The flowers, which can grow up to 3 cm above the water, are white and range in size from 18 to 25 mm [16]. *Egeria densa* has a high carbon content, consisting of 26.2% cellulose, 18.1% hemicellulose, 7.1% lignin, and 22.6% protein, along with three monosaccharides: 26.7% glucose, 5.9% galactose, and 5.1% xylose. Given its substantial carbon and carbohydrate composition, *Egeria densa* holds significant potential for various applications, and the utility of carbon quantum dots (CQDs) [17]. The use of *Egeria densa* as a precursor for the synthesis of CQDs has not been previously reported [18]. However, *Egeria densa* is used for the production of solid biofuels, such as carbon and pellets [19], so this study seeks to explore its potential in such applications.

2 Materials and Methods

2.1 *Materials*

The synthesis of S-N, CQDs involves materials: *Algae Egeria densa*, distilled water as a solvent and chemicals for the formation of S and N compounds in the form of Na_2SO_4, and NH_4OH. The manufacture of $BiVO_4$ on FTO (*fluorine-doped tin oxide*) substrate involves the following chemical materials $Bi(NO_3)_3.5H_2O$, NH_4VO_3, HNO_3, NaOH, Pretreatment of *Egeria densa* was carried out by washing the algae using running water to remove impurities and contaminants. Afterward, the algae was dried using paper towels until it was free of excess moisture, pulverized into powder, and then dissolved in a suitable solvent before being put into an autoclave for the hydrothermal process.

2.2 *Synthesis of $BiVO_4$*

The synthesis of bismuth vanadate ($BiVO_4$) starts with the preparation of a fluorine-doped tin oxide (FTO) substrate, cut to a size of 1.5 × 1 cm. Two solvent solutions are then prepared: a 2M sodium hydroxide solution and a 2M nitric acid solution, which help dissolve ammonium metavanadate and bismuth (III) nitrate. To make the precursor solution, 11,648 mg of ammonium metavanadate is dissolved in 8 mL of 2M sodium hydroxide, while 48,507 mg of bismuth (III) nitrate is dissolved in 8 mL of 2M nitric acid. The two solutions are mixed thoroughly, and concentrated nitric acid (65%) is added gradually until the pH reaches 0.9. The resulting homogeneous solution is then transferred to an autoclave containing the FTO substrate, which is placed in an oven set at 180°C for 3 h. After this stage, the sample is annealed at 450°C for 2 h.

$BiVO_4$ has two main phases, namely tetragonal (metastable) and monoclinic (stable). The monoclinic phase, which is more photocatalytically active at PEC performance, is usually more dominant at low pH. pH 0.9 creates conditions that favor controlled growth, so the resulting particles are more uniform in size and distribution which is useful for improving charge transfer efficiency across the material [20].

2.3 *Synthesis of S,N-CQDs from Egeria densa*

The process begins by washing the algae under a continuous water flow to remove dirt and impurities. Afterward, the algae are dried with tissue paper to eliminate excess moisture. Next, 3 grams of algae are carefully weighed and ground using a mortar and pestle. The resulting paste is then dissolved in a solution containing 50 mL of 5 mmol Na_2SO_4 and 50 mL of 5 mmol NH_4OH. This mixture is transferred to a Teflon-lined autoclave and heated in an oven at 250 °C for 3 h. Following this, the S,N-CQDs are filtered through filter paper and centrifuged to remove any remaining particles. The final step involves performing UV light testing to evaluate the luminescent properties of the S,N-CQDs.

2.4 *Combination of $BiVO_4$ with S,N-CQDs*

$BiVO_4$ and S,N-CQDs samples were prepared using the required equipment, including a mini compressor, airbrush spray, and hot plate. The first step was to clean the hot plate with acetone to prevent any contamination. Next, the $BiVO_4$ sample was placed on

the hot plate and heated to 100 °C during the coating process. The airbrush technique, assisted by the mini compressor, was used to spray solutions of S,N-CQDs in different volumes (2.5 mL, 5 mL, 7 mL, 7.5 mL, and 10 mL) onto the $BiVO_4$ surface from a distance of 20 cm. After spraying, the $BiVO_4$ sample was annealed at 100 °C for one hour to allow the S,N-CQDs crystals to adhere to its surface. This process was repeated with varying volumes of S,N-CQDs solution to ensure consistent results. The procedure was performed for each variation to obtain reliable and reproducible outcomes. The use of spray coating is a relatively simple and scalable method for the application of thin films on large substrates such as $BiVO_4$ and allows for a more even and consistent coating distribution [21], [22].

2.5 *Characterization of $BiVO_4$/S,N-CQDs*

The synthesized S,N-CQDs samples were characterized using UV-Vis spectroscopy (Jasco V-750) to examine their absorbance spectra and light absorption at specific wavelengths. High-Resolution Transmission Electron Microscopy (HR-TEM, 200 kV, Tecnai G2 20 S-Twin, FEI) was employed to assess the particle size distribution of the S,N-CQDs. For the $BiVO_4$/S,N-CQDs samples, UV-DRS was used to evaluate the light absorption range and the band gap energy. Field Emission Scanning Electron Microscopy (FE-SEM, Hitachi SU-3500) was utilized to study the surface morphology, shape, and size of the samples. X-ray Diffraction (XRD) analysis, performed with a Bruker D8 Advance X'Pert3 Powder and Empyrean systems using Cu Kα radiation (λ = 1.54 Å), was used to examine the crystal structure. Raman spectroscopy was applied to investigate the molecular structure and atomic vibrational modes of the samples. Photoluminescence (PL) measurements were conducted to assess charge recombination behavior and detect any defects in the samples.

2.6 *Photoelectrochemical water splitting test of $BiVO_4$/S,N-CQDs*

The photoelectrochemical water splitting test was performed to assess the material's ability to split water into hydrogen and oxygen using light energy. The tests were conducted with a 0.1 M Na_2SO_4 electrolyte solution in a three-electrode configuration. The $BiVO_4$/S,N-CQDs thin film acted as the working electrode (WE), platinum (Pt) was used as the counter electrode (CE), and Ag/AgCl served as the reference electrode (RE). A solar simulator provided the light source, with an intensity set to 100 mW/cm². Current density was measured under various conditions, including dark, bright, and with ultraviolet and infrared filters. Linear sweep voltammetry (LSV) was employed to collect data over a voltage range of –0.6 V to 1.5 V, with a minimum current threshold of 1 mA, using a PalmSens 4 potentiostat.

3 Results and Discussion

3.1 *Visual observation analysis*

Figure 1(a) shows $BiVO_4$ deposited on an FTO substrate through a straightforward hydrothermal process conducted at 180 °C for 4 h and 30 min, followed by annealing at 450 °C for 2 h. The appearance of a yellow layer on the transparent substrate confirms the successful growth of $BiVO_4$. S,N-CQDs were applied to the $BiVO_4$ surface using a spray technique from a distance of 20 cm, with the substrate placed on a hotplate. Different volumes of S,N-CQDs, namely 2.5 mL, 5 mL, 7.5 mL, and 10 mL, were used. After spraying, the surface developed a brownish-yellow color. The resulting films are shown in Figure 1(b). The color change from yellow to brownish on BiVO4 after the addition of S,N-CQDs can be attributed to the modification of the optical and electronic properties of the material due to the interaction between $BiVO_4$ and S,N-CQDs, which increases the light absorption and broadens the absorption spectrum to a longer wavelength region as supported by scientific literature [23].

Figure 2 illustrates the synthesis of S,N-CQDs from *Egeria densa* algae through a hydrothermal method at 250 °C for 3 h. The luminescent properties of the S,N-CQDs were evaluated under both visible and UV light. The S,N-CQDs emitted a cyan luminescence, which is attributed to the excitation of electrons upon UV light absorption. These excited electrons transition from the valence band to the conduction band, and upon returning to the valence band, they release energy, resulting in luminescence [24].

The photoluminescence (PL) test is related to the transition from the excited state to the ground state. In Figure 3, the S,N-CQDs sample PL test was carried out using a 450 nm filter to determine the maximum emission wavelength produced by S,N-CQDs. The result of the photoluminescence test (Figure 3) shows that the emission curve is in the green color range of 495–570 nm with the acquisition of an emission peak at 532 nm, so it can be concluded that the synthesized

S,N-CQDs produce cyan luminescence (Figure 2(b)) when S,N-CQDs are irradiated under UV light [25], [26].

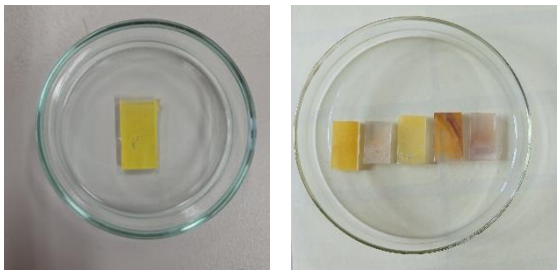

(a) (b)

Figure 1: (a) $BiVO_4$, (b) $BiVO_4$ and $BiVO_4$/S,N-CQDs.

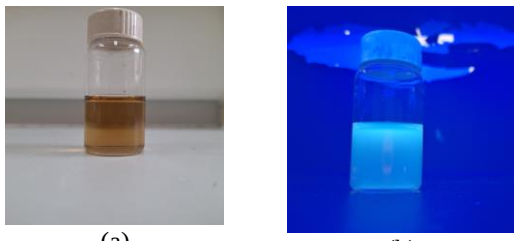

(a) (b)

Figure 2: S,N-CQDs under irradiation of (a) visible light and (b) UV light.

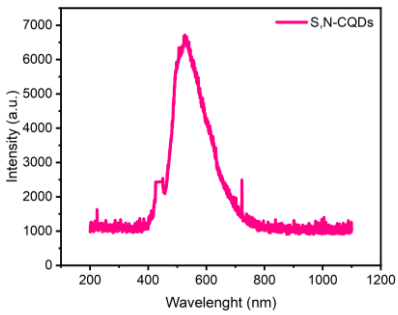

Figure 3: Photoluminesence spectrum of S,N-CQDs.

3.2 *Band gap analysis*

Figure 4(a) shows the UV-Vis absorption spectra of S,N-CQDs synthesized using the hydrothermal method. The absorption peak observed between 216–258 nm is associated with the carbon core, characteristic of aromatic benzenoid rings, primarily arising from the π-π* electronic transitions in C=C bonds. Another peak, found in the 300–350 nm range, is attributed to n-π* transitions involving C-N, C=S, and C=O bonds. The relatively low intensity of the n-π* absorption suggests a lower concentration of functional groups and reduced electron transitions in the S,N-CQDs. These findings are consistent with previous UV-Vis studies [27], [28].

Figure 4(b) illustrates the impact of incorporating S,N-CQDs on the light absorption characteristics of $BiVO_4$. The $BiVO_4$/S,N-CQDs composite exhibits increased absorption in the visible spectrum, in contrast to pure $BiVO_4$, which shows limited absorption in this range. This enhancement in light absorption is likely to improve the efficiency of the photoelectrochemical water splitting process, as reflected by the shift in the band gap.

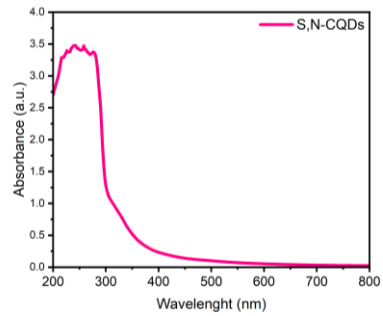

(a)

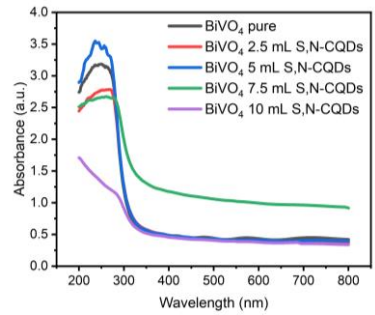

(b)

Figure 4: (a) UV-Vis spectrum of S,N-CQDs, (b) $BiVO_4$ and $BiVO_4$/S,N-CQDs.

Figure 5 displays the energy band gaps of the $BiVO_4$/S,N-CQDs samples, calculated from the UV-Vis absorption data. The band gap energies were estimated through analysis using a Tauc plot. The UV-Vis wavelength and absorbance data were transformed into an energy curve following the Tauc method to determine the band gaps. Each sample's band gap calculation was conducted using the Tauc equation, as represented in Equation (1).

$$(\alpha h\nu)^n = A(h\nu - E_g) \quad (1)$$

Where α is the absorbance coefficient, h is the Plack costant, v is the frequency, A is the absorbance data, Eg is the band gap energy and n is a power value that depends on the type of material used.

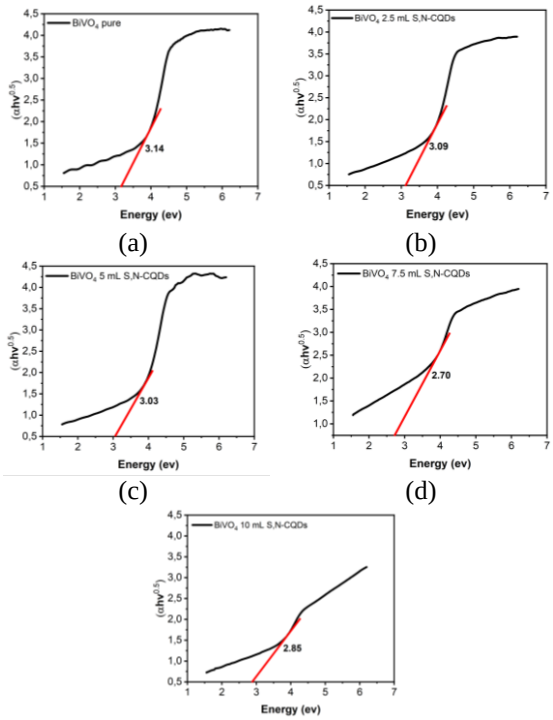

Figure 5: Tauc Plot of (a) $BiVO_4$, (b) $BiVO_4$ 2.5 mL S,N-CQDs, (c) $BiVO_4$ 5mL S,N-CQDs, (d) $BiVO_4$ 7.5 mL S,N-CQDs, (e) $BiVO_4$ 10 mL S,N-CQDs.

Figure 5 show the Tauc equation results, providing the estimated band gaps for the $BiVO_4$ samples. The pure $BiVO_4$ sample has a band gap of 3.14 eV, while the samples modified with 2.5 mL, 5 mL, 7.5 mL, and 10 mL of S,N-CQDs show band gaps of 3.09 eV, 3.03 eV, 2.70 eV, and 2.85 eV, respectively. The addition of S,N-CQDs to $BiVO_4$ effectively reduces the band gap, which enhances its absorption of visible light and boosts its photoelectrochemical performance. $BiVO_4$ can crystallize into three primary forms: monoclinic scheelite ($BiVO_4$ m-s), tetragonal zircon ($BiVO_4$ t-z), and tetragonal scheelite ($BiVO_4$ t-s), with band gaps of 2.4 eV, 2.34 eV, and 2.90 eV, respectively [29]. The band gap of pure $BiVO_4$ in this study is higher than those reported in previous research [8], [30].

3.3 *Crystallinity*

The $BiVO_4$/S,N-CQDs crystals grown on the FTO substrate were analyzed using XRD, as shown in Figure 6. The XRD data, processed with HighScore Plus software, reveal diffraction peaks at (040), (220), and (042) in the samples. Notably, the addition of S,N-CQDs improves the $BiVO_4$ sample, especially at the (002) diffraction peak. This observation is consistent with previous research suggesting that N-CQDs produce a broad, low-intensity peak at (002) with a carbon diffraction index [31].

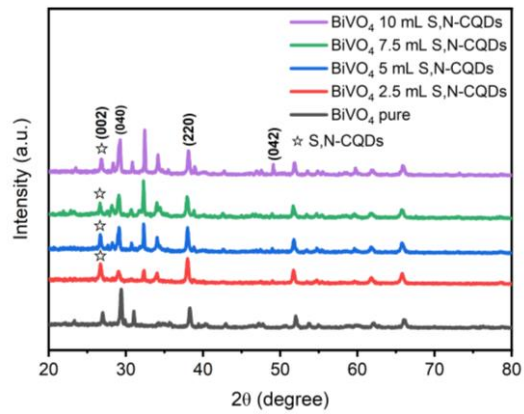

Figure 6: XRD of $BiVO_4$ and $BiVO_4$/S,N-CQDs.

From the XRD characterization data, the crystal size can be estimated using the Debye Scherrer method [32] as shown in Equation (2).

$$D = \frac{K\lambda}{\beta\cos(\theta)} \tag{2}$$

where λ= X-ray wavelength, θ= diffraction angle, K= is a constant or crystal form factor, and β= nilai full width at half maximum (FWHM). Thus the value of crystal size D and strain (Table 1) can be calculated through the Williamson-Hall method, with the following Equation (3):

$$\beta cos(\theta) = \frac{K\lambda}{D} + 4\varepsilon sin(\theta) \tag{3}$$

Table 1: Crystal sizes and strains.

Sample	Crystal Size (nm)	Strain
$BiVO_4$ pure	26.482	0.041
$BiVO_4$ 2.5 mL S,N-CQDs	20.161	2.698
$BiVO_4$ 5 mL S,N-CQDs	28.769	0.038
$BiVO_4$ 7.5 mL S,N-CQDs	25.733	0.043
$BiVO_4$ 10 mL S,N-CQDs	32.205	5.929×10^{-4}

3.4 *Morphology*

The HRTEM image of the S,N-CQDs material shown in Figure 7(a) demonstrates that the synthesized nanoparticles exhibit a uniform spherical shape and are uniformly distributed. The HRTEM analysis indicates that the average particle diameter is approximately 4.5 nm, which aligns with findings from previous studies on the properties of S,N-CQDs [26], [33], [34].

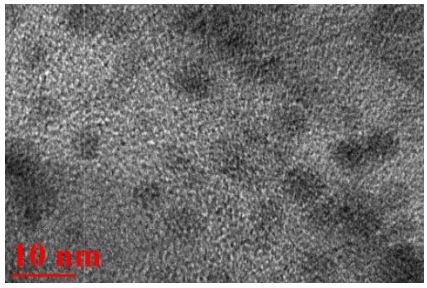

(a)

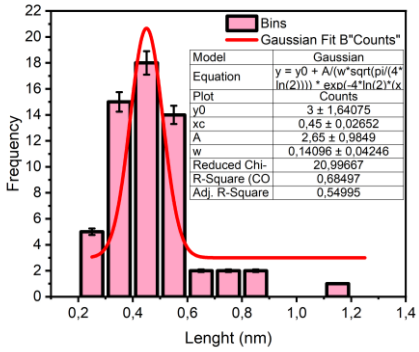

(b)

Figure 7: (a) HRTEM image of S,N-CQDs sample, (b) particle size distribution of S,N-CQDs.

Figure 8(a) and (b) show the formation of the $BiVO_4$ nanosheet structure on the FTO substrate, as observed from a top perspective and cross-section. The microplates have a minimum size ranging from 0.010 µm to a maximum size of 0.185 µm, and the film thickness, measured from the cross-section, is 0.649 µm. FESEM analysis showed an uneven distribution of the $BiVO_4$ material, with noticeable particle agglomeration. Particle size analysis, performed using ImageJ software and processed into histogram data, is shown in Figure 8(c), with a mean value size of 0.01575 µm with a standard error of 0.00126. Compared to previous studies reporting $BiVO_4$ on FTO substrates with a size of 22–25 nm [34], the current results show smaller particles. Nonetheless, the FESEM images confirm the presence of similar nanosheet structures [20].

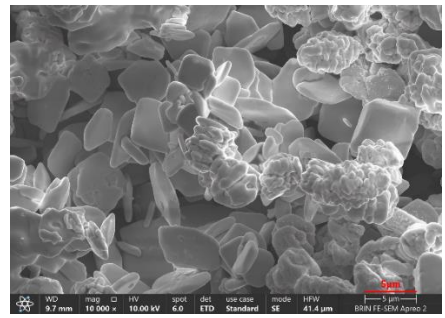

(a)

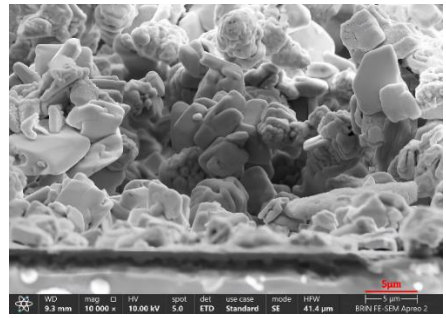

(b)

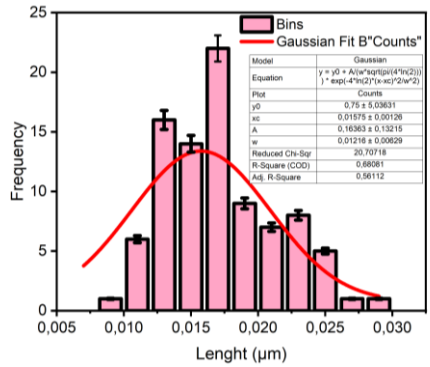

(c)

Figure 8: FESEM characterization results of (a) $BiVO_4$ image with 10,000 times magnification from a top view, (b) $BiVO_4$ image from a cross-sectional view, (c) particle size distribution of $BiVO_4$.

3.5 *Optical property*

The measurement was conducted to investigate charge recombination dynamics and identify defects in the sample. Figure 9 displays the photoluminescence (PL) results for $BiVO_4$ samples with varying volumes of S,N-CQDs (2.5 mL, 5 mL, 7.5 mL, and 10 mL) under

325 nm excitation. Overall, the inclusion of S,N-CQDs in the $BiVO_4$ samples appears to enhance charge recombination, possibly due to an increase in crystal defects [35].

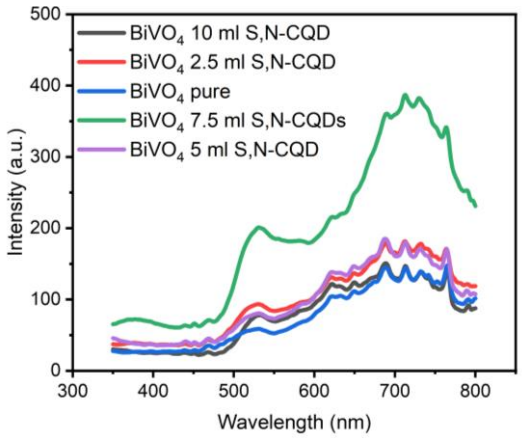

Figure 9: Photoluminescence spectra of $BiVO_4$ and $BiVO_4$/S,N-CQDs.

3.6 *Surface analysis*

Figure 10 shows the Raman spectroscopy results, which were used to examine the molecular structure and atomic vibrational modes of each sample. The spectra confirm the presence of monoclinic scheelite $BiVO_4$. The most prominent peak, located at 829 cm^{-1}, corresponds to the asymmetric stretching of the VO_4 tetrahedra. Peaks at 369 cm^{-1} and 331 cm^{-1} are associated with the bending vibrations of the VO_4 tetrahedra, while the peak at 219 cm^{-1} corresponds to crystal lattice vibrations (external mode). These results are consistent with previously reported data for monoclinic scheelite $BiVO_4$ [36], [37].

3.7 *Analysis of PEC water splitting performance*

The $BiVO_4$/S,N-CQDs samples were subjected to electrochemical testing in a 0.5 M Na_2SO_4 solution, using an Ag/AgCl reference electrode and a platinum (Pt) counter electrode. This test aimed to evaluate their catalytic performance for the hydrogen evolution reaction (HER). The external voltage was varied between –0.6 V and 1.5 V under both illuminated and dark conditions, with a solar simulator used as the light source.

3.7.1 *Linear sweep voltammetry (LSV)*

The initial parameter assessed is Linear Sweep Voltammetry (LSV), with the results shown in Figure 11. The onset potential, which indicates the voltage needed for the catalyst to achieve a specific current density, is determined from the LSV curve. Under dark conditions, the LSV measurements reveal a low current density (J_ph), indicating the lack of charge carriers that are usually generated by light. However, under illumination, the current density increases in direct proportion to the applied external bias.

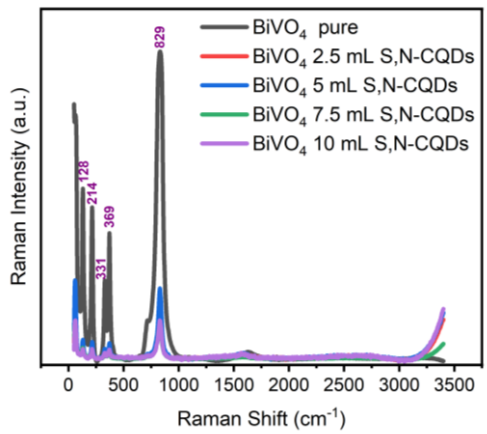

Figure 10: Raman spectra of $BiVO_4$ and $BiVO_4$/S,N-CQDs.

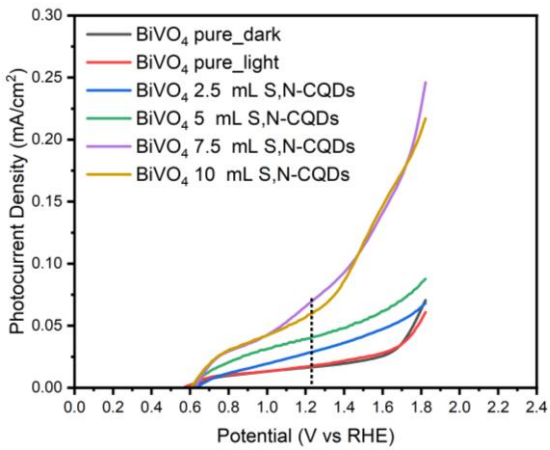

Figure 11: Linear Sweep Voltammetry (LSV) of $BiVO_4$ and $BiVO_4$/S,N-CQDs V vs Ag/RHE.

As illustrated in Figure 11, the addition of 7.5 mL of S,N-CQDs significantly enhances photoelectrochemical activity, resulting in a current density of 0.0698 mA/cm² at 1.23 V vs. RHE under

100 mW/cm² illumination. In contrast, $BiVO_4$ without S,N-CQDs exhibits a current density of approximately 0.0174 mA/cm². With 2.5 mL, 5 mL, and 10 mL of S,N-CQDs, the current densities increase to 0.0295 mA/cm², 0.0409 mA/cm², and 0.0593 mA/cm², respectively. These results indicate that the addition of 7.5 mL of S,N-CQDs enhances the visible light absorption of $BiVO_4$, thereby improving its photoelectrochemical performance. However, a subsequent test showed a decrease in current density, likely due to the dissolution of the $BiVO_4$/S,N-CQDs composite in the Na_2SO_4 solution.

Previous research shows that pure $BiVO_4$ achieves a current density of 0.035 mA/cm² at 1.23 V vs. RHE in a pH 1 solution [35]. With the addition of CQDs, this value increases to 0.47 mA/cm² at the same voltage [38]. A further improvement is seen when CQDs are combined with $CdIn_2S_4$ and $BiVO_4$, resulting in a current density of 4.84 mA/cm² at 1.23 V vs. RHE [9]. These differences in performance are attributed to variations in the $BiVO_4$ preparation methods, the incorporation of S,N-CQDs, and the experimental conditions used in each study.

3.7.2 Applied bias photon-to-current efficiency (ABPE)

Figure 12 shows the Applied Bias Photon-to-Current Efficiency (ABPE) plot, where the ABPE value is derived from the LSV data. A higher ABPE value indicates a more efficient conversion of light energy into electrical current. The ABPE is calculated using Equation (4).

$$ABPE = \frac{J_{ph} \times (1{,}23V - V_b)}{P} \times 100\% \quad (4)$$

Where Vb is E (V vs. RHE) and P is the light intensity used, which in this experiment is 100 mW cm^{-2}.

The results show that the ABPE of $BiVO_4$ with 7.5 mL of S,N-CQDs is relatively high, indicating good efficiency and superior performance compared to the other samples. The ABPE for $BiVO_4$ with 7.5 mL of S,N-CQDs is 0.0131%, followed by 0.0127%, 0.0091%, and 0.0052% for $BiVO_4$ with 10 mL, 5 mL, and 2.5 mL of S,N-CQDs, respectively. The pure $BiVO_4$ sample exhibits the lowest ABPE at 0.0047%.

Previous research has shown an ABPE of 0.02% for pure $BiVO_4$ at pH 1 [20]. The addition of CQDs boosted the ABPE to 0.21% [39], and further enhancement was observed with the CQDs/$CdIn_2S_4$/$BiVO_4$ composite, which achieved an ABPE of 1.13% [9]. The ABPE values in this study are relatively lower than those reported in the literature, with the highest value being 0.21%. These differences can be attributed to variations in the synthesis methods employed.

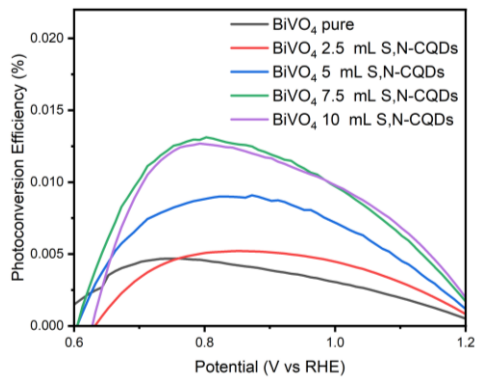

Figure 12: ABPE results of $BiVO_4$ and $BiVO_4$/S,N-CQDs.

3.7.3 Chronoamperometry (CA)

Figure 13 illustrates the chronoamperometric behavior of $BiVO_4$, both with and without the incorporation of S,N-CQDs. Chronoamperometry is a technique used to monitor the current over time under a constant applied potential, providing valuable insights into the durability and stability of the $BiVO_4$/S,N-CQDs material during the photoelectrochemical (PEC) water splitting process. The CA test was performed using an on/off cycle with 60-second intervals for a total of 420 s. The resulting data indicates the material's stability; a steady current or minimal fluctuations suggest good stability. The chronoamperometric results reveal that $BiVO_4$ with 7.5 mL of S,N-CQDs exhibited the highest stability and current, followed by pure $BiVO_4$ (0 mL of S,N-CQDs), 5 mL, and 10 mL of S,N-CQDs. The lowest stability was observed in the sample with 2.5 mL of S,N-CQDs. Modification of $BiVO_4$ with CQDs significantly improved the efficiency of charge separation and electron transfer, which in turn contributed to the enhancement of its photocatalytic activity [23].

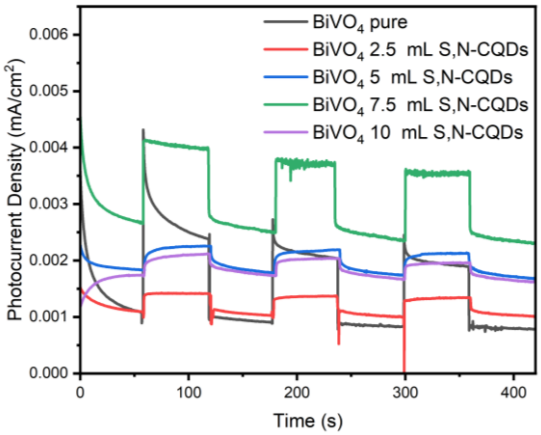

Figure 13: Chronoamperometry results of $BiVO_4$/S,N-CQDs with 0.8 Volt vs Ag/AgCl.

3.7.4 Cyclic voltammetry (CV)

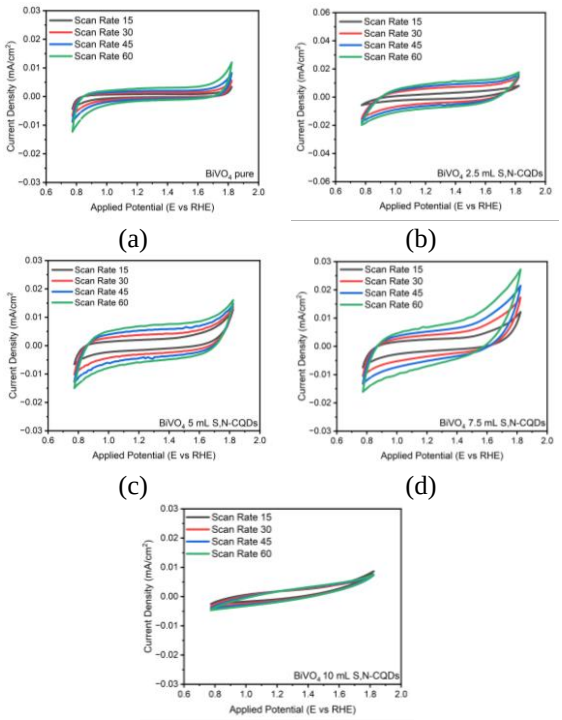

Figure 14: CV results (a) $BiVO_4$/S,N-CQDs 0 mL S,N-CQDs, (b) $BiVO_4$/S,N-CQDs 2.5 mL S,N-CQDs, (c) $BiVO_4$/S,N-CQDs 5 mL S,N-CQDs, (d) $BiVO_4$/ S,N-CQDs 7.5 mL S,N-CQDs, (e) $BiVO_4$/ S,N-CQDs 10 mL S,N-CQDs.

CV is a commonly used electrochemical technique to investigate reduction and oxidation processes in materials, as well as to examine chemical reactions driven by electron transfer. During CV, the potential is varied between two preset values, and the current flowing through the circuit is recorded. For this study, a potential range of 0.15–0.2 V was applied, with scan rates of 15, 30, 45, and 60 mV/s, using Na_2SO_4 as the electrolyte.

Figure 14 displays the CV results for the samples. It is clear that the largest CV curve area corresponds to the $BiVO_4$ sample with 2.5 mL of S,N-CQDs, followed by $BiVO_4$ with 7.5 mL, 5 mL, and 10 mL of S,N-CQDs. The smallest curve area is observed for pure $BiVO_4$. To further validate these results, the CV data will be analyzed using ESCA.

3.7.5 Electrochemical active surface area (ESCA)

ECSA represents the part of the sample that interacts directly with the electrolyte solution. To confirm the findings from the CV measurements, data analysis is performed to evaluate the ECSA. The ECSA value is calculated from the double-layer capacitance (Cdl) obtained from CV cycles at various scan rates, along with the specific capacitance (Cs), using Equation (5).

$$ESCA = \frac{C_{dl}}{C_s} \tag{5}$$

In this context, Cs represents the ideal capacitance of the surface, where a higher scan rate leads to a smaller diffusion layer, thereby increasing the current [40]. To further verify this, the CV data is analyzed to determine the ECSA. The Cdl value is extracted from the CV cycles at each scan rate and then analyzed using linear regression. Figure 15 presents a comparison of the ECSA values for each sample. The ECSA values for $BiVO_4$ without S,N-CQDs and with 2.5, 5, 7.5, and 10 mL of S,N-CQDs are 0.011 mF/cm², 0.148 mF/cm², 0.101 mF/cm², 0.102 mF/cm², and 0.012 mF/cm², respectively. A higher Cdl value indicates a larger active surface area, so the $BiVO_4$ sample with 2.5 mL of S,N-CQDs has the highest number of active sites among the samples.

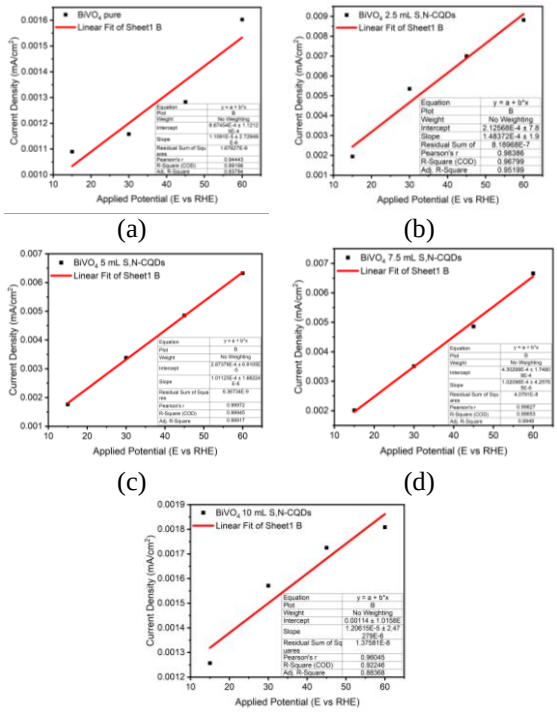

Figure 15: ESCA results (a) $BiVO_4$/S,N-CQDs 0 mL S,N-CQDs, (b) $BiVO_4$/S,N-CQDs 2.5 mL S,N-CQDs, (c) $BiVO_4$/S,N-CQDs 5 mL S,N-CQDs, (d) $BiVO_4$/ S,N-CQDs 7.5 mL S,N-CQDs, (e) $BiVO_4$/ S,N-CQDs 10 mL S,N-CQDs.

4 Conclusions

$BiVO_4$, synthesized through the hydrothermal method, exhibits a nanosheet structure with an average microplate size of 0.01575 µm and a film thickness of 0.649 µm when viewed cross-sectionally. The S,N-CQDs, also produced via hydrothermal synthesis, have a spherical shape with an average size of 4.5 nm. The use of natural precursors for S,N-CQDs (such as *Egeria densa*) provides advantages in terms of sustainability and cost.

In the LSV test for photocurrent density, the incorporation of S,N-CQD into $BiVO_4$ led to a marked increase in current density, with the most significant increase observed when 7.5 mL of S,N-CQD was added, resulting in a current density of 0.0698 mA/cm² and an ABPE value of 0.0131%, when compared to pure $BiVO_4$ which had a value of 0.0174 mA/cm² with an ABPE of 0.0047%. The higher current density indicates more efficient electron transfer from the valence band to the conduction band, enhancing hydrogen production.

The chronoamperometry data revealed that the material exhibited the highest stability with the addition of 7.5 mL of S,N-CQDs. Furthermore, the presence of S,N-CQDs induced morphological changes in $BiVO_4$, including thinner nanosheets and increased spacing between them. The addition of S,N-CQDs showed an increase in photoelectrochemical efficiency, material stability, and light absorption capability confirmed through UV-Vis testing and band gap reduction from 3.14 eV to 2.70 eV.

This study highlights the novel integration of S,N-CQDs derived from *Egeria dens*a into $BiVO_4$ photoanodes, offering a sustainable and cost-effective approach to enhance PEC performance. The reduction in band gap and improved electron transfer efficiency represent significant advancements in solar-driven hydrogen production technology. Further development can focus on optimizing the composition of S,N-CQDs and refining the synthesis methods to achieve even greater efficiency and stability. Additionally, exploring the integration of $BiVO_4$/S,N-CQDs into more complex and scalable photoelectrochemical systems could accelerate its potential for industrial applications.

Acknowledgements

We would like to express our gratitude to the Universitas Pertamina – Universiti Teknologi PETRONAS Joint Research Program for their support, through research grant number 123/UP-R/SK/HK.01/VI/2023.

Author Contributions

H.A.: methodology, investigation, research design, data analysis, writing an original draft, writing-reviewing and editing. L.R.: methodology, investigation, data curation, research design, data analysis. N.S.S.: conceptualization, methodology, investigation, reviewing and editing; data analysis, funding acquisition, project administration. V.F.: conceptualization, data analysis. S.S.: methodology, project administration; S.A.P.: research design, project administration; R.V.: conceptualization, project administration. Y.F.B.: funding acquisition, project administration. All authors have read and agreed to the published version of the manuscript.

Conflicts of Interest

The authors declare no conflict of interest.

References

[1] A. M. M. I. Qureshy, M. Ahmed, and I. Dincer, "Performance assessment study of photo-electro-chemical water-splitting reactor designs for hydrogen production," *International Journal of Hydrogen Energy*, vol. 44, no. 18, pp. 9237–9247, Apr. 2019, doi: 10.1016/j.ijhydene.2019.01.280.

[2] A. M. Abdalla, S. Hossain, O. B. Nisfindy, A. T. Azad, M. Dawood, and A. K. Azad, "Hydrogen production, storage, transportation and key challenges with applications: A review," *Energy Conversion and. Management*, vol. 165, pp. 602–627, Jun. 2018, doi: 10.1016/j.enconman.2018.03.088.

[3] B. C. Tashie-Lewis and S. G. Nnabuife, "Hydrogen production, distribution, storage and power conversion in a hydrogen economy - A technology review," *Chemical Engineering Journal Advances*, vol. 8, Nov. 2021, Art. no. 100172, doi: 10.1016/j.ceja.2021.100172.

[4] M. El Ouardi, A. El Idrissi, M. Arab, M. Zbair, H. Haspel, M. Saadi, and H. Ait Ahsaine, "Review of photoelectrochemical water splitting: From quantitative approaches to effect of sacrificial agents, oxygen vacancies, thermal and magnetic field on (photo)electrolysis," *International Journal of Hydrogen Energy*, vol. 51, pp. 1044–1067, Jan. 2024, doi: 10.1016/j.ijhydene.2023.09.111.

[5] M. G. Walter, E. L. Warren, J. R. McKone, S. W. Boettcher, Q. Mi, E. A. Santori, and N. S. Lewis, "Solar water splitting cells," *Chemical Reviews*, vol. 110, no. 11, pp. 6446–6473, Nov. 2010, doi: 10.1021/cr1002326.

[6] M. Kumar, B. Meena, P. Subramanyam, D. Suryakala, and C. Subrahmanyam, "Recent trends in photoelectrochemical water splitting: The role of cocatalysts," *NPG Asia Materials*, vol. 14, no. 1, p. 88, Dec. 2022, doi: 10.1038/s41427-022-00436-x.

[7] P. Mane, I. V. Bagal, H. Bae, A. N. Kadam, V. Burungale, J. Heo, S. W. Ryu, and J. S. Ha, "Recent trends and outlooks on engineering of $BiVO_4$ photoanodes toward efficient photoelectrochemical water splitting and CO_2 reduction: A comprehensive review," *International Journal of Hydrogen Energy*, vol. 47, no. 94, pp. 39796–39828, Dec. 2022, doi: 10.1016/j.ijhydene.2022.09.146.

[8] M. Tayebi and B. K. Lee, "Recent advances in $BiVO_4$ semiconductor materials for hydrogen production using photoelectrochemical water splitting," *Renewable and Sustainable Energy Reviews*, vol. 111, pp. 332–343, Sep. 2019, doi: 10.1016/j.rser.2019.05.030.

[9] J. Wang, T. Zhou, Y. Zhang, L. Li, C. Zhou, J. Bai, J. Li, H. Zhu, and B. Zhou, "Type-II heterojunction $CdIn_2S_4$ /$BiVO_4$ Coupling with CQDs to improve PEC water splitting performance synergistically," *ACS Applied Materials & Interfaces*, vol. 14, no. 40, pp. 45392–45402, Oct. 2022, doi: 10.1021/acsami.2c12618.

[10] R. Atchudan, S. H. Kishore, T. N. J. I. Edison, S. Perumal, R. Vinodh, A. K. Sundramoorthy, R. S. Babu, M. Alagan, and Y. R. Lee, "Highly fluorescent carbon dots as a potential fluorescence probe for selective sensing of ferric ions in aqueous solution," *Chemosensors*, vol. 9, no. 11, p. 301, Oct. 2021, doi: 10.3390/chemosensors9110301.

[11] R. Liu, J. Zhang, M. Gao, Z. Li, J. Chen, D. Wu, and P. Liu, "A facile microwave-hydrothermal approach towards highly photoluminescent carbon dots from goose feathers," *RSC Advances*, vol. 5, no. 6, pp. 4428–4433, 2015, doi: 10.1039/ C4RA12077A.

[12] D. Yao, A. Liang, and Z. Jiang, "A fluorometric clenbuterol immunoassay using sulfur and nitrogen doped carbon quantum dots," *Microchimica Acta*, vol. 186, no. 5, p. 323, May 2019, doi: 10.1007/s00604-019-3431-8.

[13] Y. Park, K. J. McDonald, and K. S. Choi, "Progress in bismuth vanadate photoanodes for use in solar water oxidation," *Chemical Society Reviews*, vol. 42, no. 6, pp. 2321–2337, 2013, doi: 10.1039/C2CS35260E.

[14] P. Casati, M. V. Lara, and C. S. Andreo, "Induction of a C4-Like Mechanism of CO_2 fixation in *Egeria densa*, a submersed aquatic species," *Plant Physiology*, vol. 123, no. 4, pp. 1611–1622, Aug. 2000, doi: 10.1104/pp.123.4.1611.

[15] U.S. Fish and Wildlife Service. "Ecological risk screening summary Brazilian waterweed." fws.gov. https://www.fws.gov/sites/default/files/documents/Ecological-Risk-Screening-Summary-Brazilian-Waterweed.pdf (accessed May 31, 2015).

[16] M. Yarrow, V. H. Marín, M. Finlayson, A. Tironi, L. E. Delgado, and F. Fischer, "The ecology of *Egeria densa* planchón (Liliopsida:

Alismatales): A wetland ecosystem engineer?," *Revista Chilena de Historia Natural*, vol. 82, no. 2, Jun. 2009, doi: 10.4067/S0716-078X2009000200010.

[17] C. G. De Azevedo, R. J. Dos Santos, C. T. Hiranobe, A. F. Zanette, A. E. Job, and M. J. Silva, "The invasive *Egeria densa* macrophyte and its potential as a new renewable energy source: A study of degradation kinetics and thermodynamic parameters," *Science of The Total Environment*, vol. 856, Jan. 2023, Art. no. 158979, doi: 10.1016/j.scitotenv.2022.158979.

[18] L. Cui, X. Ren, M. Sun, H. Liu, and L. Xia, "Carbon dots: Synthesis, properties and applications," *Nanomaterials*, vol. 11, no. 12, p. 3419, Dec. 2021, doi: 10.3390/nano11123419.

[19] X. Álvarez, Á. Cancela, V. Freitas, E. Valero, Á. Sánchez, and C. Acuña-Alonso, "Hydrothermal carbonization and pellet production from *Egeria densa* and *Lemna minor*," *Plants*, vol. 9, no. 4, p. 425, Mar. 2020, doi: 10.3390/plants9040425.

[20] Y. Miao, J. Liu, L. Chen, H. Sun, R. Zhang, J. Guo, and M. Shao, "Single-atomic-Co cocatalyst on (040) facet of $BiVO_4$ toward efficient photoelectrochemical water splitting," *Chemical Engineering Journal*, vol. 427, Jan. 2022, Art. no. 131011, doi: 10.1016/j.cej.2021.131011.

[21] C. Wang, X. Lin, C. G. Schäfer, S. Hirsemann, and J. Ge, "Spray synthesis of photonic crystal based automotive coatings with bright and angular-dependent structural colors," *Advanced Functional Materials*, vol. 31, no. 9, Feb. 2021, Art. no. 2008601, doi: 10.1002/adfm.202008601.

[22] S. I. Park, Y. J. Quan, S. H. Kim, H. Kim, S. Kim, D. M. Chun, C. S. Lee, M. Taya, W. S. Chu, and S. H. Ahn, "A review on fabrication processes for electrochromic devices," *International Journal of Precision Engineering and Manufacturing*, vol. 3, no. 4, pp. 397–421, Oct. 2016, doi: 10.1007/ s40684-016-0049-8.

[23] C. Hu, Q. Chen, M. Tian, W. Wang, J. Yu, and L. Chen, "Efficient combination of carbon quantum dots and $BiVO_4$ for significantly enhanced photocatalytic activities," *Catalysts*, vol. 13, no. 3, p. 463, Feb. 2023, doi: 10.3390/ catal13030463.

[24] Y. A. Asmara, A. R. Maharani, L. S. Aulia, and I. A. D. Astuti, "Perbandingan sifat optik cdots berbahan daun binahong (*anredera scandes l.*) segar dan kering menggunakan metode bottom up," *Jurnal Inovasi Penelitian dan Pembelajaran Fisika*, vol. 3, no. 2, 2022, doi: 10.26418/jippf. v3i2.56837.

[25] R. Behnood and G. Sodeifian, "Novel $ZnCo_2O_4$ embedded with S, N-CQDs as efficient visible-light photocatalyst," *Journal of Photochemistry and Photobiology A: Chemistry*, vol. 405, Jan. 2021, Art. no. 112971, doi: 10.1016/j.jphotochem. 2020.112971.

[26] O. A. Aladesuyi and O. S. Oluwafemi, "Synthesis of N, S co-doped carbon quantum dots (N,S-CQDs) for sensitive and selective determination of mercury (Hg^{2+}) in *Oreochromis niloctus* (Tilapia fish)," *Inorganic Chemistry Communications*, vol. 153, Jul. 2023, Art. no. 110843, doi: 10.1016/j.inoche.2023.110843.

[27] Y. Deng, J. Qian, Y. Zhou, and F. Lu, "Regulatory preparation of N/S Doped carbon quantum dots and their applications as Fe(III) ion sensors," *ChemistrySelect*, vol. 5, no. 17, pp. 5306–5311, May 2020, doi: 10.1002/slct.202000039.

[28] T. Teymoorian, N. Hashemi, M. H. Mousazadeh, and Z. Entezarian, "N, S doped carbon quantum dots inside mesoporous silica for effective adsorption of methylene blue dye," *SN Applied Sciences*, vol. 3, no. 3, p. 305, Mar. 2021, doi: 10.1007/s42452-021-04287-z.

[29] G. Li, Y. Bai, and W. F. Zhang, "Difference in valence band top of $BiVO_4$ with different crystal structure," *Materials Chemistry and Physics*, vol. 136, no. 2–3, pp. 930–934, Oct. 2012, doi: 10.1016/j.matchemphys.2012.08.023.

[30] H. Nezzal, S. Rahmane, E. G. Temam, M. Al-Abri, H. H. Kyaw, B. Gasmi, M. Althamthami, H. B. Temam, and J. Hu, "Photo-deposition of AgO thin films on TiO_2 substrate for (P-N) hetero-junction applications: Considering the degree of contamination," *Journal of Alloys and Compounds*, vol. 1010, Jan. 2025, Art. no. 177331, doi: 10.1016/j.jallcom.2024.177331.

[31] F. Qin, Y. Ma, S. Zheng, C. Hu, L. Wei, R. Yang, Y. Ma, and C. Zhang, "Construction of novel Z-Scheme N-CQDs/Sn_3O_4 heterojunction for excellent photocatalytic degradation of organic pollutant," *Journal of Cluster Science*, vol. 33, no. 3, pp. 913–923, May 2022, doi: 10.1007/ s10876-021-02020-9.

[32] M. Sumadiyasa and I. B. S. Manuaba, "Determining crystallite size using Scherrer formula, Williamson-Hull plot, and particle size with SEM," *Buletin Fisika*, vol. 19, no. 1, p. 28, Jul. 2018, doi: 10.24843/BF.2018.v19.i01.p06.

[33] T. Liu, Z. Cui, J. Zhou, Y. Wang, and Z. Zou, "Synthesis of pyridinic-rich N, S co-doped carbon quantum dots as effective enzyme

mimics," *Nanoscale Research Letters*, vol. 12, no. 1, p. 375, Dec. 2017, doi: 10.1186/s11671-017-2149-y.

[34] X. Cao, Y. Gu, H. Tian, Y. Fang, D. Johnson, Z. Ren, C. Chen, and Y. Huang, "Microemulsion synthesis of ms/tz-$BiVO_4$ composites: The effect of pH on crystal structure and photocatalytic performance," *Ceramics International*, vol. 46, no. 13, pp. 20788–20797, Sep. 2020, doi: 10.1016/j.ceramint.2020.05.048.

[35] L. Chen, S. F. Yin, R. Huang, Q. Zhang, S. L. Luo, and C. T. Au, "Hollow peanut-like m-$BiVO_4$: facile synthesis and solar-light-induced photocatalytic property," *CrystEngComm*, vol. 14, no. 12, p. 4217, 2012, doi: 10.1039/c2ce06684j.

[36] P. Brack, J. S. Sagu, T. A. N. Peiris, A. McInnes, M. Senili, K. G. U. Wijayantha, F. Marken, and E. Selli, "Aerosol-assisted CVD of bismuth vanadate thin films and their photoelectrochemical properties," *Chemical Vapor Deposition*, vol. 21, no. 1-2-3, pp. 41–45, Mar. 2015, doi: 10.1002/cvde.201407142.

[37] F. F. Abdi and R. van de Krol, "The nature and light-dependence of bulk recombination in co-pi catalyzed $BiVO_4$ photoanodes," *Journal of Physical Chemistry C*, vol. 116, no. 17, pp. 9398-9404, Apr. 2012, doi: 10.1021/jp3007552.

[38] P. C, J. Schuch, B. Kaiser, and W. Jaegermann, "The determination of electrochemical active surface area and specific capacity revisited for the system MnO_x as an oxygen evolution catalyst," *Zeitschrift für Physikalische Chemie*, vol. 234, no. 5, pp. 979–994, May 2020, doi: 10.1515/zpch-2019-1514.

[39] T. Zhou, S. Chen, J. Wang, Y. Zhang, J. Li, J. Bai, and B. Zhou "Dramatically enhanced solar-driven water splitting of $BiVO_4$ photoanode via strengthening hole transfer and light harvesting by co-modification of CQDs and ultrathin β-FeOOH layers," *Chemical Engineering Journal*, vol. 403, Jan. 2021, Art. no. 126350, doi: 10.1016/j.cej.2020.126350.